JOURNAL OF GEOPHYSICAL RESEARCH, VOL. 99, NO. C5, PAGES 9907–9923, MAY 15, 1994

The eddy field associated with the Azores Front east of the Mid-Atlantic Ridge as observed by the Geosat altimeter

P.-Y. Le Traon
CLS Space Oceanography Group, Toulouse, France

P. De Mey
Groupe de Recherches de Géodésie Spatiale, Toulouse, France

Abstract. Two years of Geosat data (November 1986 to December 1988) for the Azores-Madeira region of the North Atlantic are analyzed. The objective is to study the eddy field associated with the terminal retroflection of the Azores current. The rms variability of sea level anomaly is 4 to 8 cm, with maximum values between 33° and 35°N being associated with the Azores current and located on its northern flank. Higher energy is observed during winter and during the year November 1987 to November 1988. Analysis of velocities at crossovers reveals anisotropy with larger meridional velocity variances. This is the signature of meanders and/or eddies elongated in the north-south direction. The eddy-mean flow interaction is studied through the analysis of the Reynolds tensor. Meridional and zonal accelerations of the mean by the eddy field are consistent with retroflection of the Azores Current to the south and to the west. Spectral analyses show that the dominant signals have periods and wavelengths larger than 100 days and 300 km, respectively. Propagation velocities are westward but slow (1.5 km/d). Synoptic mapping of the eddy field shows the wavelike structure of the variability on the northern flank of the current. It is likely that the wave generation is not directly due to an instability of the Azores current but is attributable to a cause more to the east. Once formed, the wave interacts with the current in winter and forms meanders. Seasonal variations of the surface circulation are finally analyzed from the 2-year-long time series of synoptic maps. There is a clear seasonality in the surface circulation which generally appears to be consistent with historical in situ measurements. In winter there is a strong meandering and a southward branching, while in summer the mean front is narrower and penetrates further to the east.

1. Introduction

Two years of Geosat altimeter data were used to study the mean and variable ocean circulation in the Azores-Madeira region (27°–37°N, 18°–30°W). This study is a contribution to the SEMAPHORE program [*Eymard et al.*, 1991]. Our Azores-Madeira study area contains the eastern part of the North Atlantic subtropical gyre, and the general circulation is dominated by the eastward flowing Azores current and its recirculation first to the south and then to the west. The Azores current is characterized by strong temperature and salinity cross-gradients, which are the signature of the well-known "Azores front." The Azores current west of the Mid-Atlantic ridge is the extension of the southeast branch of the Gulf Stream [*Gould*, 1985]. It crosses the ridge between 32° and 37°N, near the Oceanographer and Hayes fracture zones. The current flows across the eastern basin at about 34°N and has three main southward recirculation branches which join the westward flowing North Equatorial current [*Klein and Siedler*, 1989]. These branches, which vary seasonally and interannually [e.g., *Stramma and Siedler*, 1988], are found just east of the Mid-Atlantic Ridge, in the central basin (our study area), and near the coast of western Africa. However, the apparent continuity of the Azores front from the western to the eastern basin as portrayed in mean circulation maps [e.g., *Klein and Siedler*, 1989] conceals significant differences. West of 30°W, the front is limited southward by the 18°C water of the Sargasso Sea, and there is little variation in Mediterranean water through the front. On the other hand, east of 30°W, the front is no longer bounded on its southern side by 18°C water and the Mediterranean water has been observed only on its northern side [*Gould*, 1985; *Sy*, 1988]. In addition, this continuity is not confirmed by the near-synoptic view of the ocean circulation obtained during the Topogulf experiment (P.-Y. Le Traon and M. Ollitrault, The Azores front west of the Mid-Atlantic Ridge, as observed from Lagrangian and hydrographic measurements, unpublished manuscript, 1992). The Azores front seems thus to be an intermittent feature, meandering and embedded in mesoscale eddies and moving over time. It is narrow (between 50 and 100 km wide). However, its intermittent occurrence implies net eastward transport smoothed out in latitude by its lateral displacements.

Mesoscale circulation in the Azores-Madeira region is therefore dominated by the meandering of the Azores front/current and by its associated eddies [e.g., *Käse and Siedler*,

Paper number 93JC03513.
0148-0227/94/93JC-03513$05.00

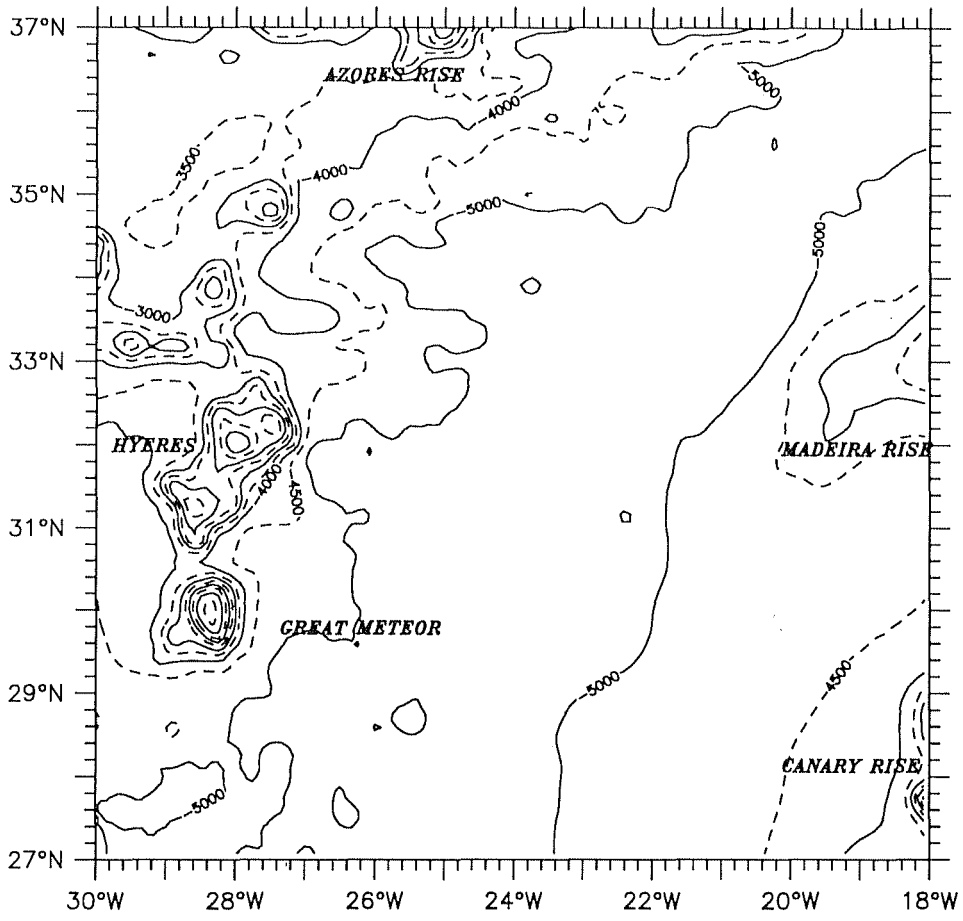

Figure 1. Bottom relief in the study domain. Contour interval is 500 m.

1982; *Käse et al.*, 1985, 1986]. There are some numerical and observational reasons to think that part of this mesoscale variability may result from the baroclinic instability of the Azores current [*Käse et al.*, 1985; *Kielmann and Käse*, 1987; *Spall*, 1990]. At depths where the Mediterranean tongue is found (between 800 and 1300 m), meddies can be a major source of variability [*Armi and Zenk*, 1984]. *Stramma and Siedler* [1988] have also detected seasonal variations of the circulation in this part of the subtropical gyre. They observe the strengthening of the Azores current in summer and an axis shift of about 2° to the south.

Analyzing mesoscale variability in this part of the subtropical gyre is important to understanding the generating mechanisms. The fact is that eddy-resolving models such as the Community Modeling Experiment are very poor at mapping this variability [*Spall*, 1990; *Böning and Budich*, 1991], even at high spatial resolutions. The capabilities and original contribution of the Geosat altimeter [*Cheney et al.*, 1987] for observing mesoscale circulation, even in regions of low eddy energy, are now well established [see *Le Traon*, 1992, for a review]. Satellite altimetry thus provides a unique tool for investigating the mesoscale variability associated with the Azores current. In addition, satellite altimetry provides a quantitative constraint to statistical and dynamical models [e.g., *De Mey*, 1992], but it is essential to evaluate the physical contents of the measurement prior to performing assimilation in a model. *Tokmakian and Challenor* [1993] have performed a first general analysis of Geosat data for the Canary basin. They showed the wavelike structure of the mesoscale variability associated with the Azores front. We will focus here on a smaller domain, which allows for a more detailed analysis.

Our study domain is the Azores-Madeira region in the northeast Atlantic (27°–37°N, 18°–30°W). Figure 1 shows the bottom relief in the domain. It is characterized by an abyssal plain oriented NE-SW and about 5300 m deep in its center. The eastern boundary was chosen so as to intersect the Madeira rise at 33°N and the Canary rise at 27°–29°N. The abyssal plain rises up to the NW corner. Very large seamounts can be seen at 28°–29°W between 29° and 35°N. Along the northern boundary the bottom slopes up rather abruptly to the north; the bathymetric structure is almost zonal. Figure 2 shows the dynamic height at 125 m with reference to 3000 m, calculated from the *Robinson et al.* [1979] (hereinafter referred to as RBS) annual atlas data. The near-surface geostrophic current pattern is dominated by an eastward flowing jet with velocities up to 6 cm/s. The jet splits into two branches at 32°N, 23°W: the southern branch recirculates to the west, and the eastern branch leaves the analysis domain on the northern flank of the Madeira rise.

Standard techniques used to process altimeter data are summarized in section 2. We start our analysis with a general statistical description of sea level variability and its seasonal and interannual variations. Results are given in section 3.

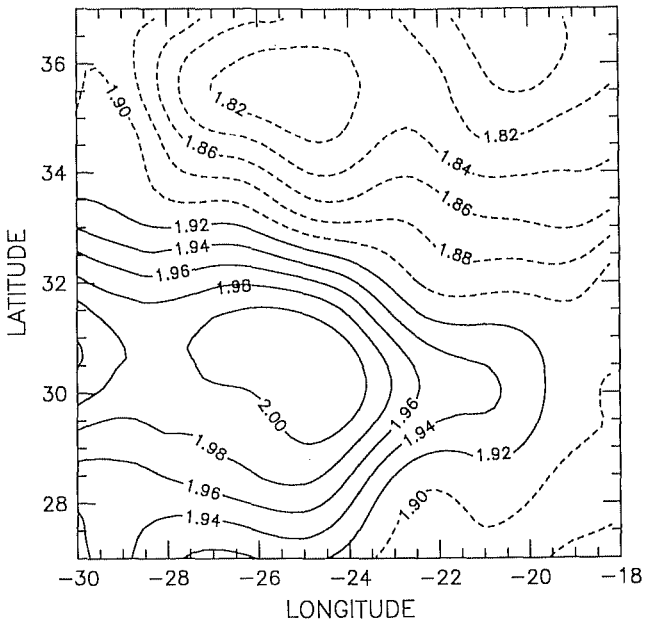

Figure 2. Climatology of the study domain. Annual 125-m dynamic height is relative to 3000 m as from *Robinson et al.* [1979]. Contour interval is 0.02 dynamic meters.

They are complemented in section 4 by wavenumber and frequency/wavenumber spectral analyses which yield the dominant space and time scales of the mesoscale variability. Eddy-mean flow interactions determined from the Reynolds tensor components are analyzed in section 5. Section 6 presents objectively analyzed synoptic maps of the eddy field and their seasonal averages. Conclusions are given in section 7.

2. Data Processing

Two years of Geosat data, for November 1986 to December 1988, were processed. We used the Geosat GEMT-2 precise orbit, characterized by an rms error of 30–40 cm [*Haines et al.*, 1990]. A total of 44 17.05-day cycles were processed (Figure 3). We used 2500-km-long tracks centered on the study domain. The tracks are long enough for the radial orbit error to be removed efficiently without significantly affecting the oceanic signal of interest here.

We calculated the altimeter residuals using the conventional repeat-track method [e.g., *Le Traon et al.*, 1990]. We briefly summarize it here. The corrections available in the Geophysical Data Record (GDR) were first applied: 2% of $H_{1/3}$, Fleet Numerical Oceanography Center (FNOC) dry and wet tropospheric corrections, ionospheric corrections from the Global Positioning System climate model, Melchior Earth tides, and Schwiderski ocean tides. We did not correct for the inverse barometer effect. The GDR data were interpolated by a cubic spline function with 10-km steps to obtain regular along-track sampling and identical sample locations for each pass. We then calculated the variations relative to the mean profile on each track. Orbit error was modeled and removed by fitting a first-degree polynomial to individual tracks. The polynomial fit takes into account the nonhomogeneity of the mesoscale variability by using the signal variance to weight the individual measurements [*Le Traon et al.*, 1991]. However, the results obtained differ only slightly (about 1 cm rms) from those using an unweighted adjustment method, as the signal is relatively homogeneous in the study area. Once the orbit error correction was applied, the

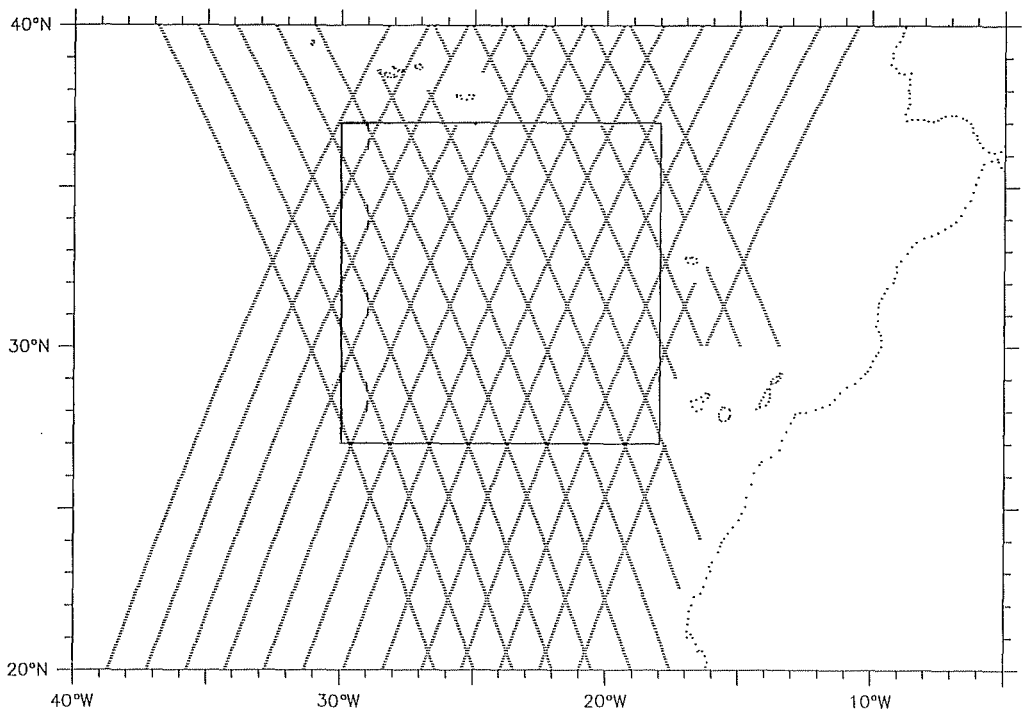

Figure 3. The Geosat tracks used in the study. The study domain is delineated by the box.

along-track sea level anomaly (SLA) data were passed through a low-pass Lanczos filter with a cutoff wavelength of 100 km.

We next endeavored to assess the advantage of using the Groupe de Recherches de Géodésies Spatiale Geosat wet tropospheric correction calculated from special sensor microwave/imager (SSMI) data [*Minster et al.*, 1992], which is thought to be considerably more accurate than the FNOC correction. For this purpose we calculated a new data set of residuals and compared it with the FNOC-corrected data set. The comparison was done for only 1 year (September 1987 to September 1988), as there are no SSMI data before September 1987. The rms discrepancy between the two data sets without polynomials fitted is typically 3–4 cm rms. However, the differences are essentially at long wavelengths and are almost completely removed after fitting a degree 1 polynomial (rms errors are between 1 and 2 cm). This result thus agrees with that of *Jourdan et al.* [1990] in confirming that the wet tropospheric correction is not really a problem for mesoscale studies in the northeast Atlantic. We thus reverted to the original FNOC correction for the rest of the study.

3. General Statistical Analysis

3.1. The rms Sea Level Anomaly

The rms SLA variability maps were obtained using the method described by *Le Traon et al.* [1990], which is as follows. The SLA data are assembled in 1°-square boxes. The variances over the boxes are then calculated along with their associated errors. The errors are estimated by assuming decorrelations of 34 days and 100 km. Before contouring, the variances and errors are smoothed by convoluting them with an isotropic Gaussian-shaped hat function with 1° standard deviation in a manner similar to objective analysis. Since this smoothing technique takes the errors into account, it preserves the statistically significant characteristics of the mapped signals.

The SLA rms variability (Figure 4) is in the range 3–8 cm. The map reveals a tongue of maximum variability centered approximately at 34°N. The latitudinal extension of the tongue decreases as one moves eastward from roughly 4° at 30°W to below 2° at 20°W. Its axis is coincident with the climatological axis of the Azores current in the western part and then separates from it to the north as a branch of the mean current veers to the south (Figure 2). This observation that the eddy field associated with the Azores front is more energetic to the north of the front is in good agreement with the numerical simulations by *Kielmann and Käse* [1987].

The influence of bottom topographical features (see Figure 1) can be felt at 28°W, where seamounts (such as the Great Meteor at 29.5°N) induce a local increase in variability. This also seems to be true in the southeast corner near the Canary shelf. The influence of the bottom relief is actually much more visible on the cross-track velocity variance map (not shown), which means that the variability is characterized by small spatial scales. The maximum slope of the geoid above the Great Meteor seamount is 10 cm/km, and there may also be a cross-track gradient effect in the geoid. The rms lateral repeat errors of 500 m produce rms topography errors of 5 cm on scales typical of the geoid anomaly, i.e., 50 km. South of 31°N, part of the variability around 28°W could therefore be due to geoid gradient errors. However, further north, the signal is stronger and the geoid gradients are noticeably weaker. As a consequence, we do not think that our results are significantly contaminated by geoid gradients.

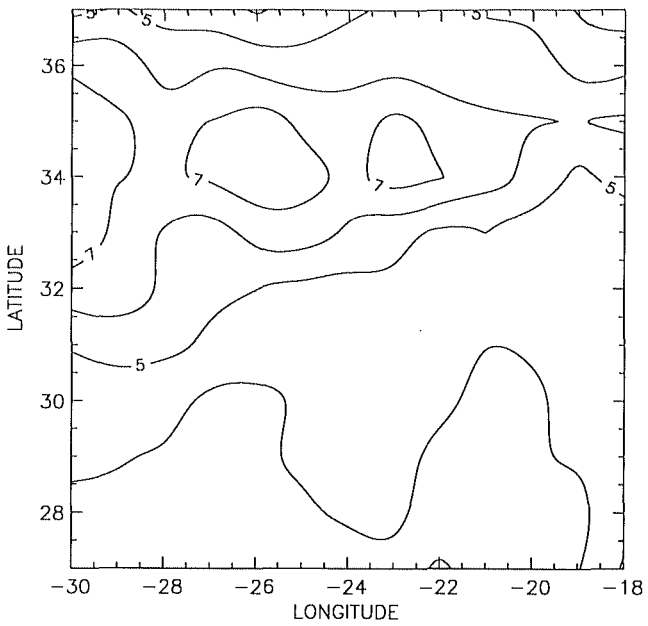

Figure 4. The rms variability of Sea Level Anomaly (SLA). Contour interval is 1 cm.

3.2. Temporal Correlations of Sea Level Anomaly

The 17-day SLA isocorrelation map (Figure 5) was obtained by calculating the one-cycle-lag temporal covariance at each measurement location along individual tracks. The mapping was performed as described in section 3.1. The formal error on these estimates, assuming a space decorrelation of 100 km, is of the order of 0.05, edges excepted. The

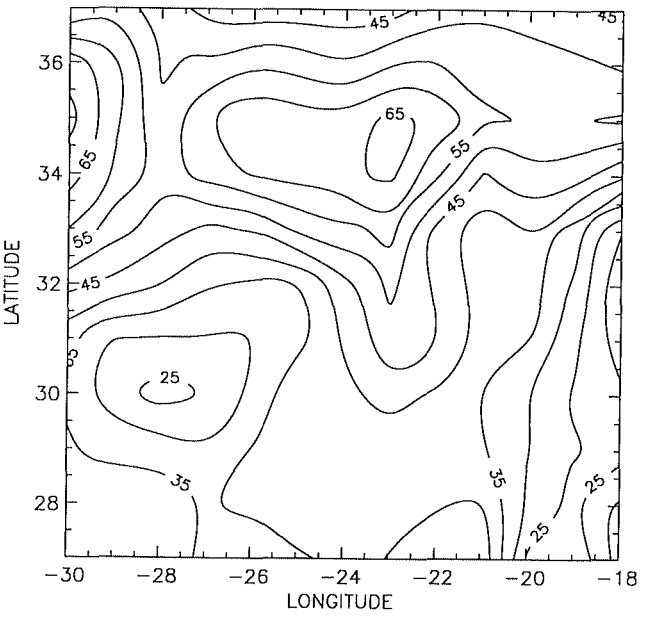

Figure 5. The 17-day isocorrelation of SLA. Contour interval is 5%.

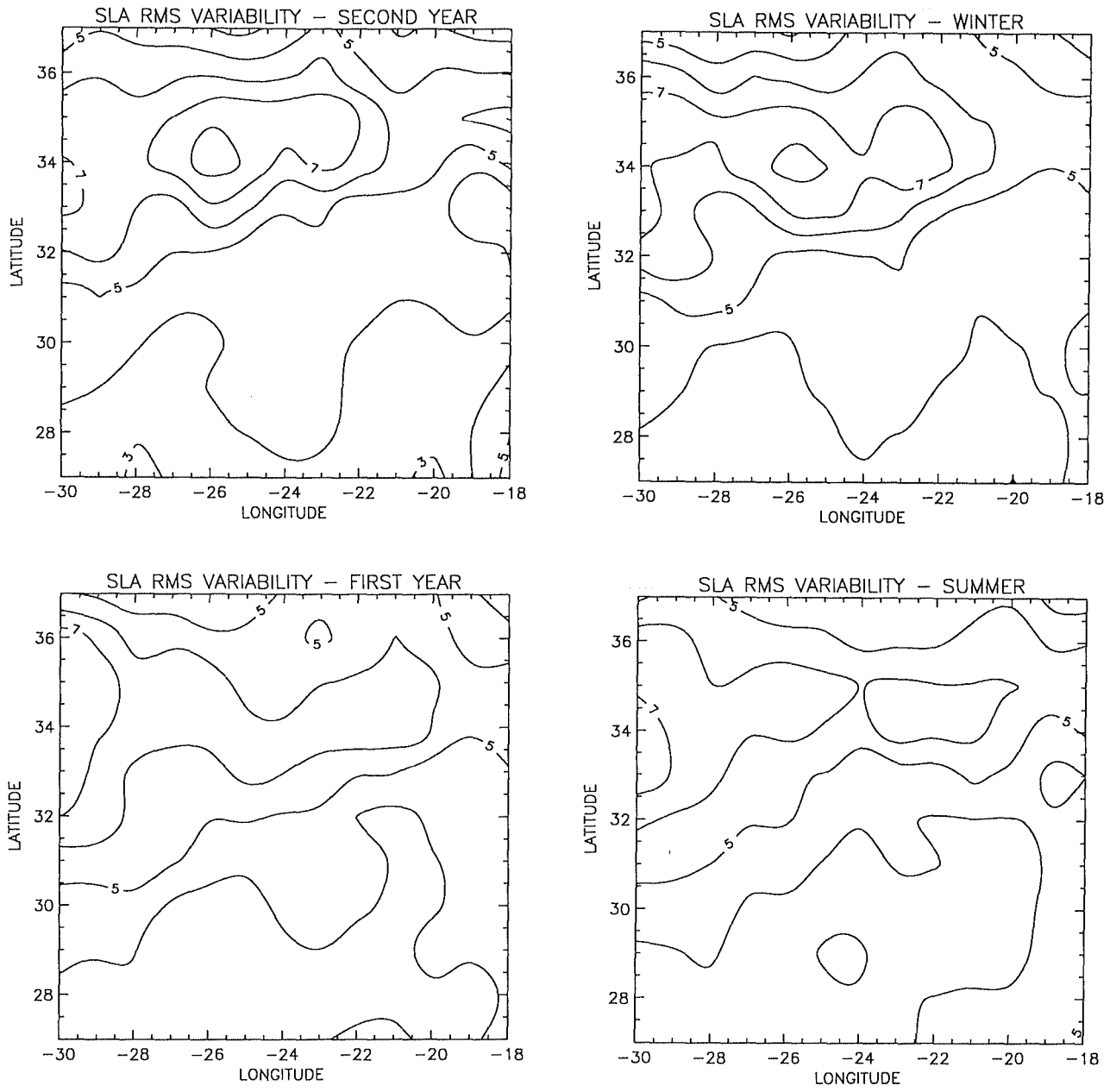

Figure 6. The rms variability of SLA for summer and winter months during the 2 years studied. Contour interval is 1 cm.

17-day correlations are between 0.25 and 0.70. The largest values (>0.60) are found in the high-variability tongue north of the statistical mean current. These values can be compared with 17-day correlations of 0.1–0.2 typically observed in areas where the Gulf Stream is the most turbulent [*Le Traon*, 1991]. The mesoscale structures associated with the Azores current are thus characterized by a high temporal coherence. The exception is the Great Meteor Seamount area (30°N–28°W), where 17-day correlations drop to 0.25. The Great Meteor area is thus characterized by small, short-lived, energetic features. The gap at 27°–28°W in the axis of the high-variability tongue is another prominent feature of the map; this apparent discontinuity may be due to the comparatively short period over which statistics are accumulated compared to the long time scales in the tongue. It may also be related to bathymetry. Finally, one can note that the 17-day correlation lines seem to follow the mean path of the Azores current, even as a branch veers to the south near 23°W, at least until it reaches 30°N.

3.3. Seasonal and Interannual Variations of SLA Statistics

We now discuss statistics accumulated separately for the winter months (October 15 through April 15) and the summer months (April 15 through October 15) on one side and separately for each of the 2 years on the other side. This gives four maps, both in terms of rms SLA (Figure 6) and SLA 17-day isocorrelation (Figure 7). (The 2-year estimates are given in Figures 4 and 5, respectively.) The seasonal and

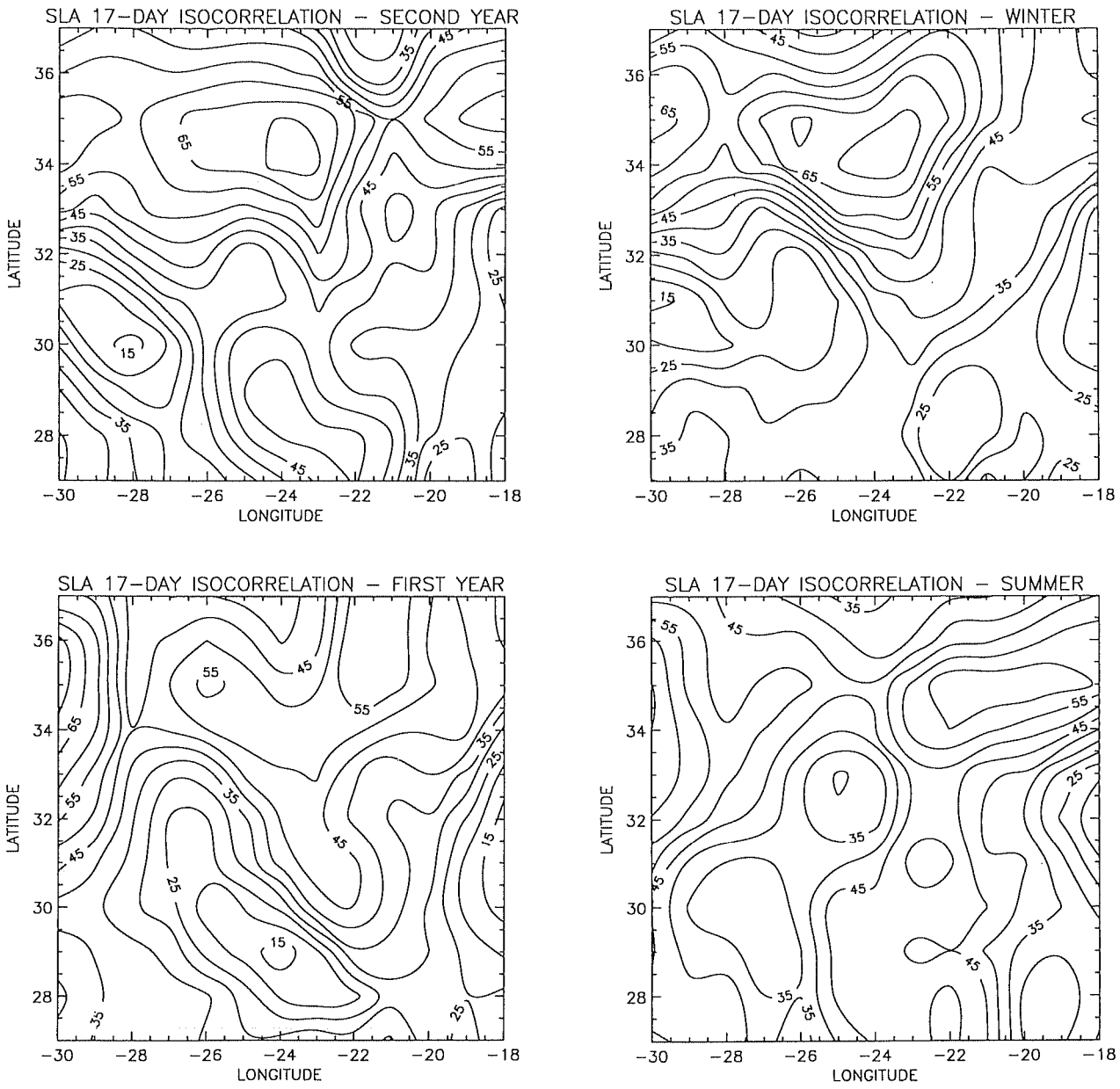

Figure 7. The 17-day isocorrelation of surface topography (SLA) for summer and winter months over the 2 years studied. Contour interval is 5%.

interannual variations are moderate but significant: the 1-standard-deviation error is below 10%. The seasonal and interannual variations are of the same order of magnitude. In the maximum variability tongue the signal is stronger during winter and during the second year. In our results the seasonal variations were consistent from one year to the next, i.e., strengthening during the winter for both years. Using a hydrological historical data set, *Klein and Siedler* [1989] observe, in contrast to our results, an increase in the eddy potential energy in the Azores front region in summer. This difference may be due to interannual variability, again keeping in mind the fact that we are looking only at a 2-year period. The tongue does not appear to move significantly in latitude. This seems to contradict the findings of *Stramma and Siedler* [1988]. Remember, however, that the axis of maximum variability probably does not directly reflect the mean circulation. In summer, the tongue extends noticeably further to the east. Figures 6 and 7 show that whenever the tongue is "active," it is also characterized by high temporal coherence. We are thus inclined to consider these characteristics as the signature of the dominant process in the tongue. From our limited data set, it seems that this dominant process is located more to the west in winter than in summer and thus that it is more strongly linked to the Azores current in winter than in summer. This observation may be put in parallel with the seasonal changes in the surface circulation noted by *Stramma and Siedler* [1988]. The seasonal changes in the surface circulation observed from Geosat will be discussed in section 6.

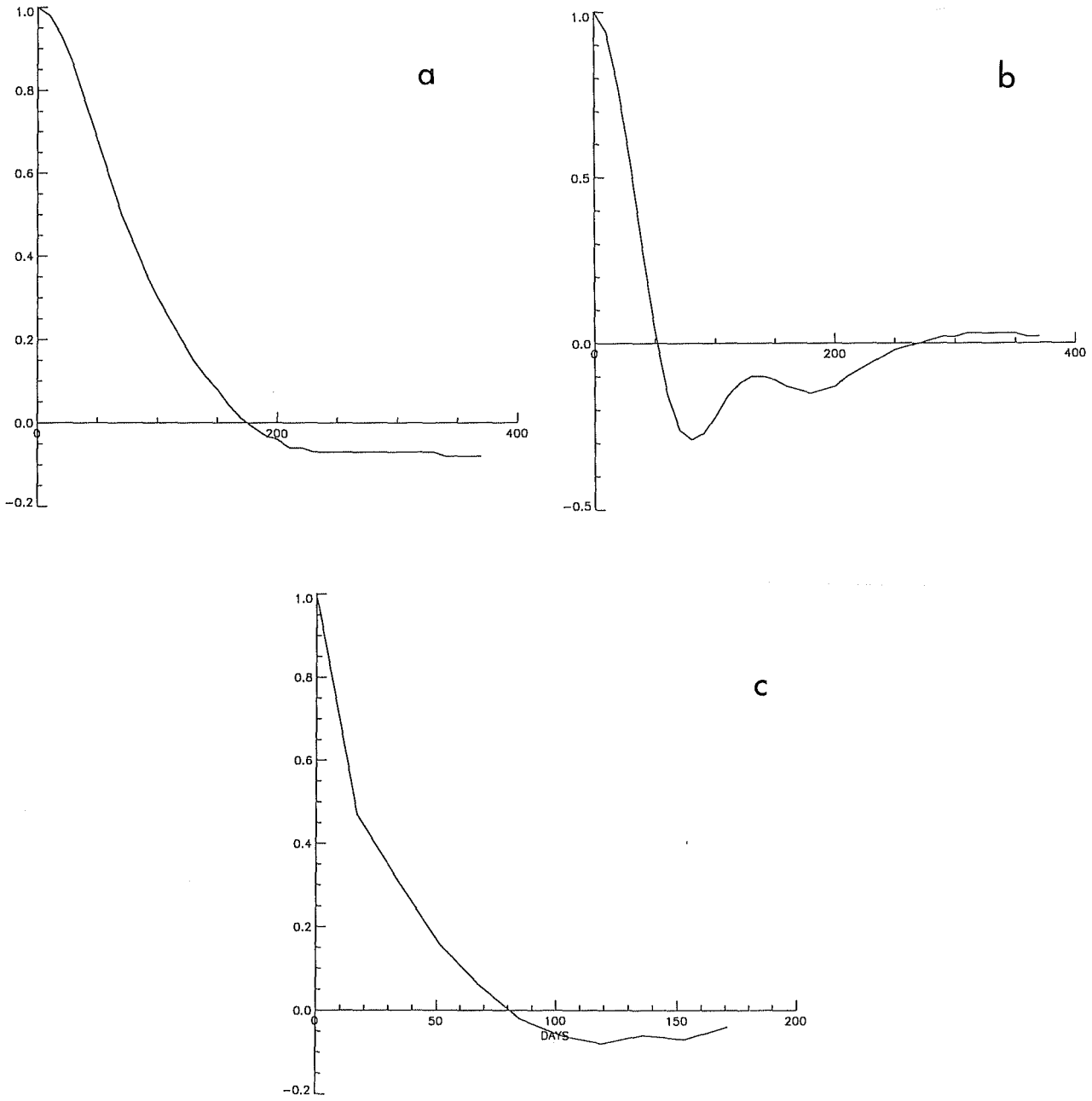

Figure 8. Mean space autocorrelation function for sea level anomaly (a), mean space autocorrelation function for transverse geostrophic velocity (b), and mean temporal autocorrelation function for sea level anomaly (c).

4. Dominant Space and Time Scales

We now present along-track spectra and autocorrelations derived from SLA data within the study area, that is, 27°–37°N, 18°–30°W. We used 17 tracks, each about 1500 km in length. Again, the methodology is given by *Le Traon et al.* [1990] and *Le Traon* [1991]. Prior to the calculations, each individual profile was detrended. Profiles with more than two consecutive missing data points and profiles shorter than 750 km were dismissed, which left about 500 profiles of an initial total of 650.

4.1. Space and Time Correlation Functions

Figure 8a shows the isotropic space autocorrelation of sea level anomaly $C(r)$ as a function of the distance r, calculated from along-track SLA data. The zero-crossing radius is 170 km. This value depends strongly on the degree of the polynomial fit to the along-track heights. In order to characterize the space scales independently of the first-degree-polynomial fit, it is advantageous to estimate the transverse velocity correlation $g(r)$ assuming horizontal nondivergence, since it is expressed as a second derivative of C in the relation $g(r) = -C''(r)$. It is shown as a function of r in Figure 8b. The distance of the first zero-crossing of g is 50 km. This value agrees with in situ observations [*Käse et al.*, 1985]. For comparison, the Rossby radius of the first baroclinic mode in the area is 27 km according to *Emery et al.* [1984].

The zero-crossing lag of the mean SLA time autocorrela-

tion function (Figure 8c) is 80 days. This is long compared to the time scales observed further north [e.g., *Mercier and Colin de Verdière*, 1985]. It also hints at the fact that any observed propagation must be slow. The long time scales are consistent with in situ measurements. Records for current meters in this area show that the energy is mainly observed for periods larger than 150 days [*Schmitz et al.*, 1988] and reveal the occurrence of strong velocity events, of the order of 30 cm/s, associated with the meandering Azores current with time scales in the range 1–3 months [*Siedler et al.*, 1985].

4.2. Wavenumber Spectra

The average wavenumber spectrum of unfiltered SLA is shown in Figure 9a. Confidence intervals were calculated assuming decorrelations of 51 days and 300 km. By choosing a decorrelation of one track in three and one cycle over three, our error estimates are thus probably conservative. The mean slope is -3, and the break in the slope occurs at 350 km. However, the spectrum stays red up to the longest observable wavelengths, that is, up to 1000 km (the slight decrease in the spectral density at 1500-km wavelength is mostly caused by the procedure used for removing the orbit error). The break in the slope occurs close to 4π, the Rossby radius of the first baroclinic mode, as already observed by *Le Traon et al.* [1990] in a more systematic study of the North Atlantic ocean. This result also agrees with quasi-geostrophic turbulence models [*Hua and Haidvogel*, 1986] which show that the nonlinear cascading of energy to the larger scales comes to a stop at a scale slightly less than twice the wavelength corresponding to the first internal Rossby radius. The winter months and the second year are, as expected, more energetic than the summer months and the first year, but differences are not statistically significant (Figures 9b and 9c). The differences between winter and summer are essentially at long wavelengths in the "linear part" of the spectrum. The higher noise level in winter may be due to the larger altimeter noise that is due to the rougher sea. The dominant process in the high-variance tongue consequently seems to be more closely related to wave dynamics than to a highly nonlinear eddy field.

4.3. Frequency/Wavenumber Spectra

The frequency/wavenumber spectrum was calculated with only seven tracks (four ascending and three descending); tracks with more than two consecutive missing cycles and shorter than 1 year were dismissed. The spectrum may thus not be representative of the whole area. Figure 10 shows the mean spectrum in a variance-preserving form. Assuming five independent tracks, this yields 20 degrees of freedom and a confidence interval of $\pm 40\%$ (at 90%). Energy is found at large wavelengths between 300 and 700 km and for periods longer than 100 days. This corroborates results from previous sections, namely, that the mesoscale variability associated with the Azores front is characterized by long periods and large wavelengths. There is a strong maximum in the spectrum at 250 days and about 600 km. Another maximum, although less significant, is also observed at 120 days and 300 km. Propagation spectra (not shown) indicate a clear westward propagation for these dominant signals. The 120-day signal could be the signature of eddies and meanders within the axis of the Azores current. The 250-day period signal is, however, probably not directly related to the Azores current and may correspond to Rossby waves. For a Rossby radius of 30 km, the dispersion relation for first-mode baroclinic Rossby waves yields a period of 430 days for a wavelength of 600 km, that is, a westward phase velocity of 1.4 km/d. The observed propagation velocity observed here is almost twice as large. However, as explained by *Le Traon* [1991], the wavelengths and propagation velocities of waves "seen" on the tracks can be overestimated by a factor of $1/\cos\theta$ (where θ is the angle between the track and the wave vector), that is, of about 2. Thus, accepting the fact that the 250-day signal has a westward propagation, its characteristics are not inconsistent with those of a baroclinic Rossby wave. Rossby waves were also detected by *Tokmakian and Challenor* [1993] in a different analysis of Geosat data for the Canary basin. They found larger dominant wavelengths of typically 800 km. We do not have a clear explanation for this difference. They were looking, however, at a much larger area than ours, and the two results are not directly comparable.

We calculated the amplitude of the 250-day signal by fast Fourier transform filtering on each along-track time series. The same calculation was performed for the annual signal. The 250-day signal and the annual signal reach a maximum in the variability region directly within the Azores front (Figures 11a and 11b). These two signals combined explain almost 40% of the total signal variance, the annual signal being slightly more energetic. The 250-day signal is mainly observed north of the Azores current and in the eastern part. Near 20°W, 35°N, it explains 25% of the signal total variance which is its largest relative contribution. In comparison, the annual signal is found more southward and westward. This suggests that the 250-day-period wave propagating westward could be slowed down by the eastward flowing mean current. The 250-day and annual period signals may also be the signatures of two distinct phenomena, although we are clearly not in a position to separate them from each other.

5. Eddy-Mean Flow Interaction

We now characterize the anisotropy of the fluctuations and their interaction with the mean flow. To this purpose we calculate the components of the Reynolds tensor at crossovers as explained by *Morrow et al.* [1992]. To reduce the noise in the subsequent calculations, each SLA pass is now run through a low-pass Lanczos filter with a cutoff wavelength of 150 km. At each crossover, the cross-track velocities for the ascending and descending tracks are then calculated. The velocities are converted to a common date by linear time interpolation. The resulting zonal and meridional velocities u' and v' are then derived by simple geometry. The components of the Reynolds tensor, that is, the variances $\langle u'^2 \rangle$ and $\langle v'^2 \rangle$ and the turbulent stresses $\langle u'v' \rangle$, are calculated by averaging over time at each crossover.

The error on the components of the Reynolds tensor depends on the cross-track velocity noise and the latitude [*Morrow*, 1992]. Given our filter characteristics and the 4 cm rms Geosat altimeter measurement noise, the cross-track velocity noise at 30°N was estimated by simulation to be about 4 cm/s (this figure is increased to 7 cm/s for a filter cutoff wavelength of 100 km). This gives meridional and zonal velocity variance noises of about 30 and 10 $cm^2\ s^{-2}$, respectively. Note that the error on the meridional velocity variance is about three times larger than that on the zonal

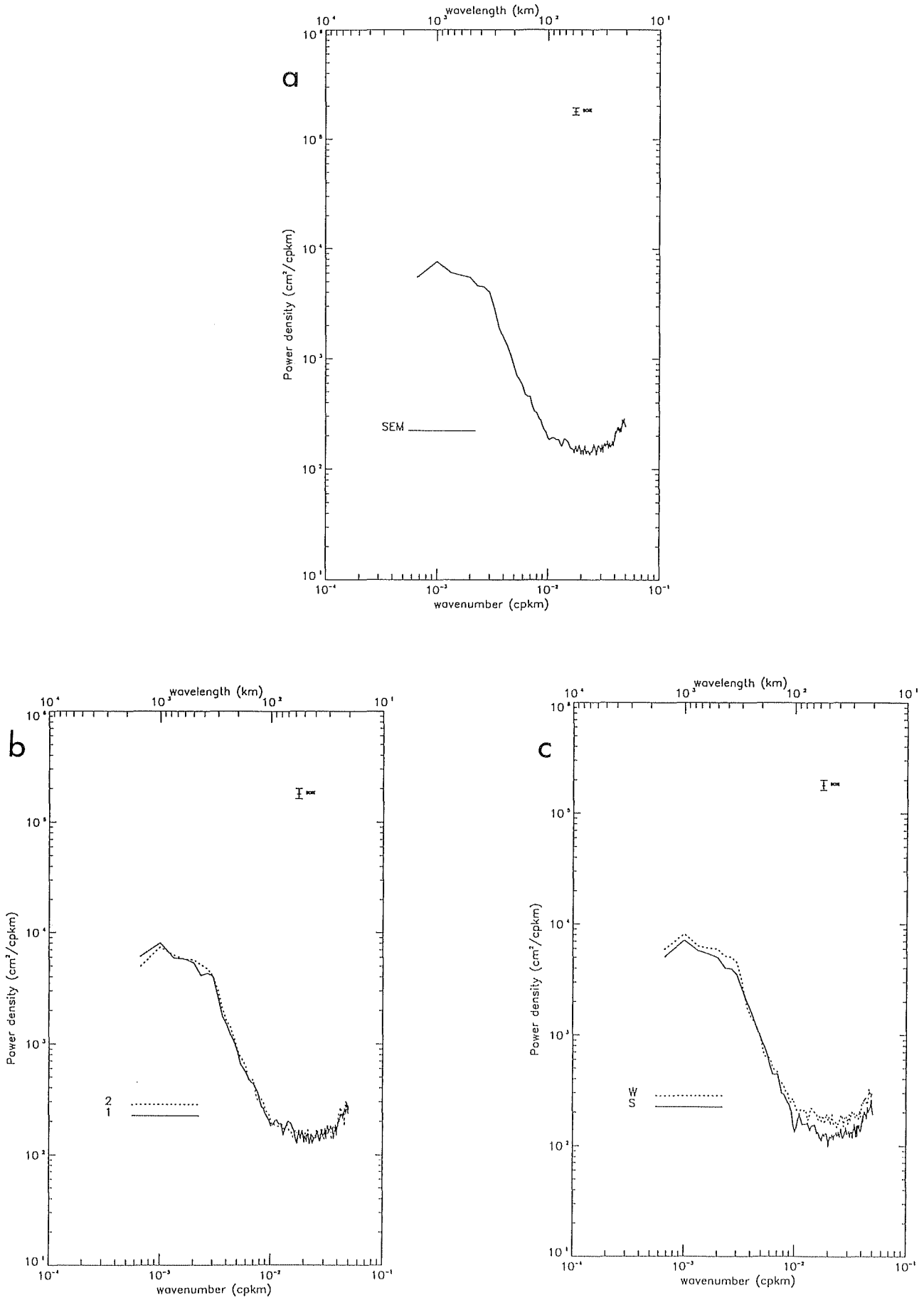

Figure 9. Wavenumber spectra shown are the mean (a), those for years 1 and 2 (b), and those for summer (S) and winter (W) months. (cpkm, cycles per kilometer).

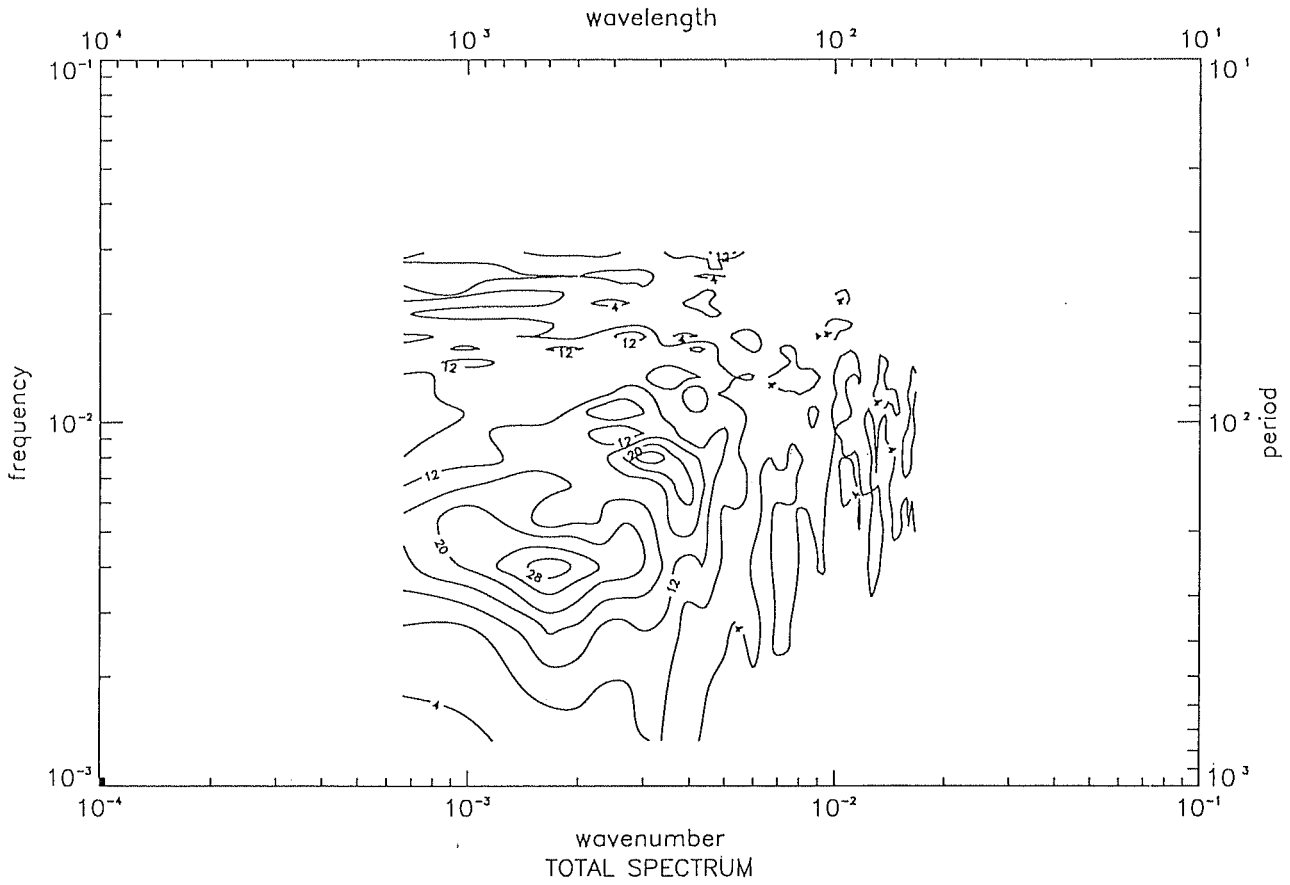

Figure 10. SLA frequency/wavenumber spectrum in variance-preserving form. Contour interval is 4 cm^2.

velocity variance because of the track orientation at 30°N [*Parke et al.*, 1987]. The time difference at crossovers can induce additional errors [*Morrow*, 1992]. However, given the high correlation of mesoscale variability in our area, especially in the high-variability tongue (see Figure 5), this error is probably marginal. Finally, the statistical significance of results must be assessed. Given the Geosat data coverage in our area, we typically get about 20–25 estimates at a given crossover point. Since we also average in space with our objective mapping procedure, we estimate the number of degrees of freedom to be at least 25. Typical statistical accuracy for variance estimates would thus be less than 30%, and according to a Fisher test, anisotropy will be significant provided the ratio v'^2/u'^2 is larger than 2.

The principal axes of variance (Figure 12), that is, the eigenvectors of the Reynolds tensor, show that the high-variance tongue north of the Azores front is characterized by strong anisotropy. In this tongue, the meridional variance (300 $cm^2\ s^{-2}$; Figure 13b) is typically three to four times larger than the zonal variance (80 $cm^2\ s^{-2}$; Figure 13a). This anisotropy is probably the signature of major meridionally oriented meanders or of meridionally elongated eddies. Given our error estimates (above), the observed anisotropy cannot be due to the higher noise level on the estimation of the meridional velocity. An upper bound for the error on the estimation of the meridional velocity can also be given by the smallest observed meridional velocity variance, which is of the order of 70 $cm^2\ s^{-2}$. Anyway, this would not explain a difference of 220 $cm^2\ s^{-2}$ between both components. Analyses of drifting buoys in the area [*Krauss and Käse*, 1984; *Krauss and Böning*, 1987; *Maillard and Käse*, 1989] show eddy kinetic energy levels of about 100 $cm^2\ s^{-2}$, in reasonable agreement with the Geosat results. However, the velocity variance measured at the Kiel 276 mooring at 33°N, 22°W [*Müller and Siedler*, 1994] at a 250-m depth is below 50 $cm^2\ s^{-2}$. We find about twice as much there. This may be due to sharp increases in velocities near the surface or to local anisotropy. Note also that, according to RBS, the mooring is in a spot where mean currents are very weak. The turbulent stresses $\langle u'v' \rangle$ (Figure 13c) range between −30 and 40 $cm^2\ s^{-2}$. They are generally negative in the north and positive in the south. As a reminder, this pattern is found in situations of baroclinic instability of a zonal jet and in situations of radiation of Rossby waves away from a zonal jet [*Ikeda*, 1981; *Flierl et al.*, 1987; *Tai and White*, 1990].

The components of the Reynolds tensor can be used to study the eddy-mean flow interaction. The contribution of the eddy field to the accelerations of the mean flow in the zonal Z and meridional M directions are given by:

$$Z = -\frac{\partial}{\partial x}\langle u'^2 \rangle - \frac{\partial}{\partial y}\langle u'v' \rangle \quad (1)$$

$$M = -\frac{\partial}{\partial y}\langle v'^2 \rangle - \frac{\partial}{\partial x}\langle u'v' \rangle \quad (2)$$

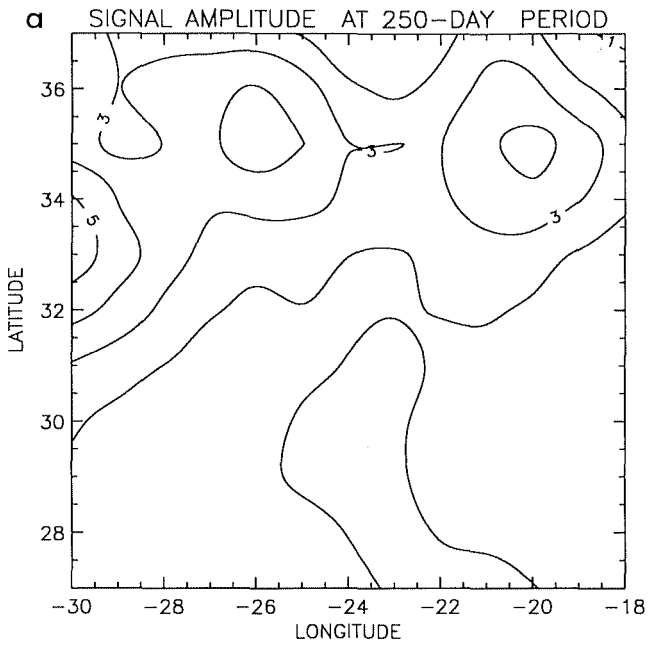

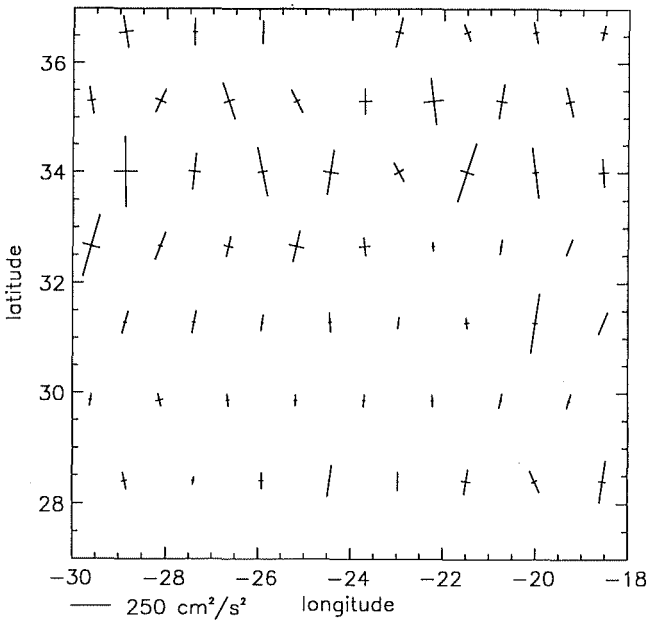

Figure 12. Principal axes of geostrophic velocity variance at crossovers.

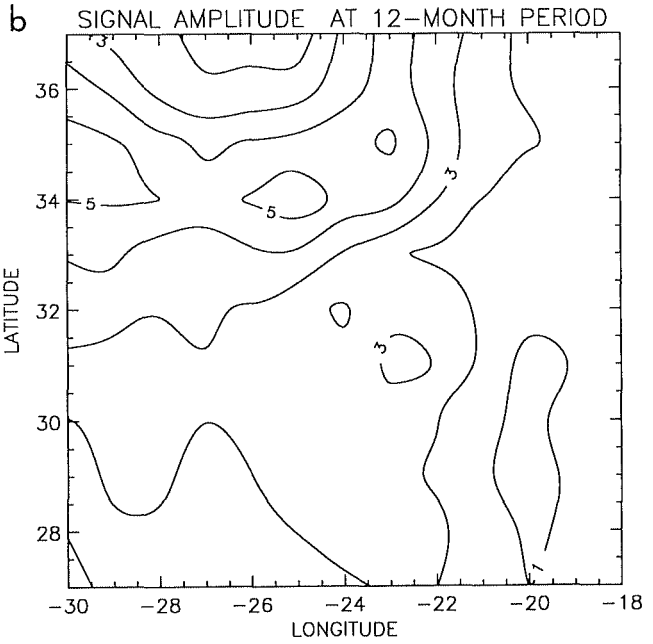

Figure 11. The rms amplitudes of signals for the 250-day period (a) and the annual period (b).

Note, however, that the divergence of the Reynolds stresses leads to an acceleration of the mean flow only if the other terms in the momentum equation are small. Z and M are shown on Figures 14a and 14b. Given the uncertainty on u' and the larger one on v' and the 2-year-only time series, their interpretation must be seen, however, as indicative only. As will be seen below, the fact that they do not appear too noisy and are oceanographically sensible probably means that they are not just noise.

Let us first have a look at the zonal acceleration term (1). Most of the structure is due to the stress term $-(\partial/\partial y)\langle u'v'\rangle$. In particular, the stress pattern implies a transfer of zonal momentum to the mean current in the westernmost part of the high-variance tongue at 34°N. In subregions located north and south, the zonal acceleration is westward, which also corresponds to a transfer to the mean current, since the current is headed westward there (Figure 2). If we follow the mean path of the Azores current from the western region where the turbulent stresses are active, we see that the zonal acceleration gradually vanishes until 23°W, where a branch of the current separates and veers to the south. East of 23°W, the eastward flowing branch is again accelerated by the turbulent field. The relative pattern of zonal acceleration by the eddy field is thus consistent with the Lagrangian acceleration of a particle entrained with the statistical mean current, at least qualitatively. This is true in particular in the case of the separation of the southern branch at 23°W, which could indicate that this separation is linked with the action of the turbulent field onto the mean.

The meridional acceleration (2) is much larger. Most of the structure now is due to the meridional gradient of $\langle v'^2\rangle$. We observe an "instability pattern" centered at 34°N. On average, a particle moving away from the 34°N latitude is accelerated in the direction of its motion. The effect is enhanced at 30°, 25°, and 22°W and is weaker in between. The axis of the instability pattern is roughly coincident with the axis of the high-variance tongue: it is coincident with the mean current in the east and then separates from it as the current flows southeastward. It is again consistent with the presence of a wave packet at 34°N. The zonal variations observed in the pattern are probably due to the slow propagation of the waves over the 2-year period. They may also be related to bathymetric effects. The other prominent feature of the meridional acceleration map is the positive acceleration at 29°N, 23°W; thus the effect of the turbulent field seems at least qualitatively to explain the retroflection of the southern branch to the west. Finally, both the zonal acceleration and the meridional acceleration terms are con-

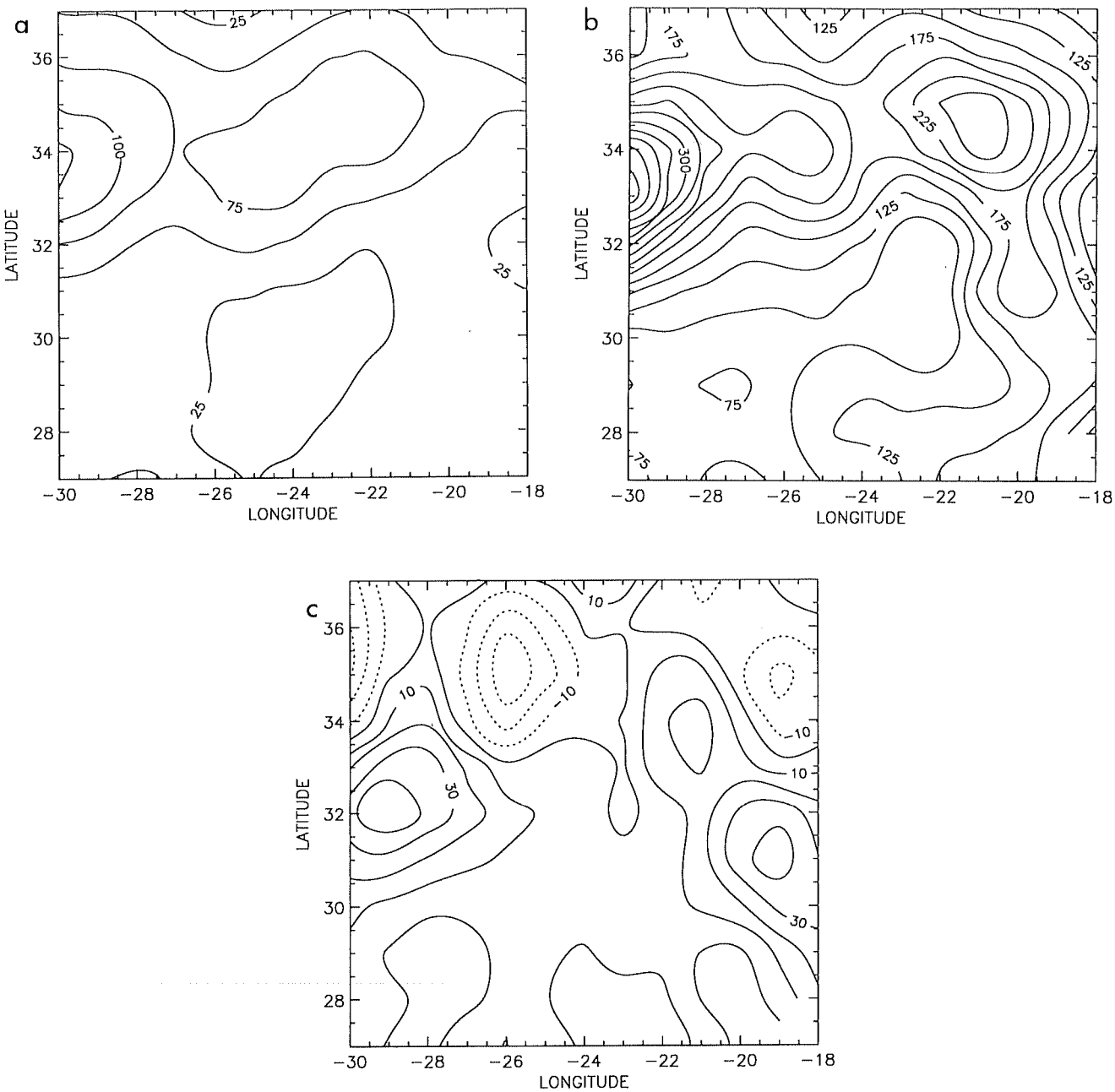

Figure 13. Reynolds tensor components $\langle u'^2 \rangle$ (a), $\langle v'^2 \rangle$ (b), and $\langle u'v' \rangle$ (c). Contour interval is 25 cm^2 s^{-2} for Figures 13a and 13b and 10 cm^2 s^{-2} for Figure 13c.

sistent with a net acceleration of the eastern branch as it reaches the eastern boundary north of the Madeira rise.

6. Synoptic and Seasonal Maps of the Eddy and Mean Field

We use the SLA data to map the two-dimensional fields by suboptimal space-time objective analysis, as was done by *De Mey and Ménard* [1989]. The space-time autocorrelation function is

$$C(r, \delta t) = [1 + ar + \tfrac{1}{6}(ar)^2 - \tfrac{1}{6}(ar)^3] \exp\left(-ar - \frac{\delta t^2}{R_t^2}\right) \quad (3)$$

as given by *Arhan and Colin de Verdière* [1985] and *Le Traon and Hernandez* [1992], where $a = 2.1038$ is chosen so that $C(1, \delta t) = 0$. The nondimensional radius r is given by

$$r^2 = \frac{(\delta x - c_x \delta t)^2}{R_x^2} + \frac{(\delta y - c_y \delta t)^2}{R_y^2} \quad (4)$$

as a function of the space and time increments δx, δy, and δt; space and time correlation radii R_x, R_y, and R_t; and propagation c_x and c_y. Here we chose 160 km, 200 km, and 60 days and (−1.5 and −0.3 cm/s). These values were determined by visually fitting (3) to the tabulated SLA space-time correlations. Note that in comparison to the previous Reynolds stress analysis, the calculation of corre-

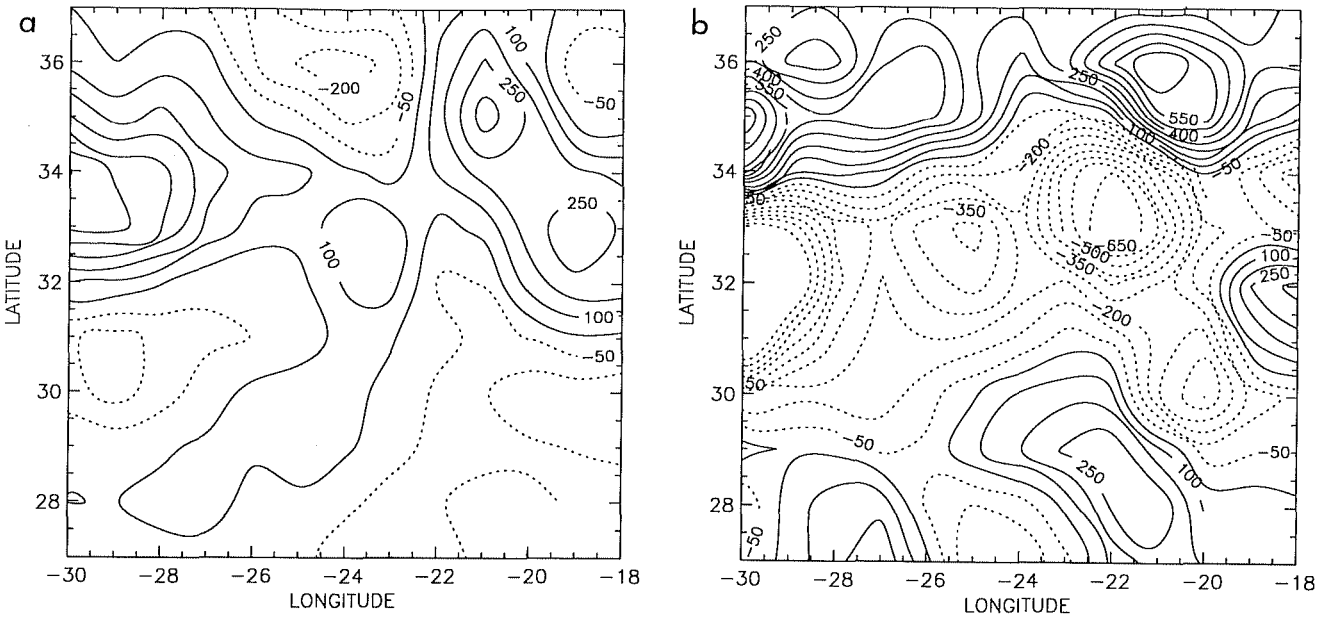

Figure 14. Mean flow acceleration by zonal (a) and meridional (b) fluctuations. Contour interval is 75 10^{-6} m s^{-2}.

lation functions assumes spatial homogeneity and the estimation of the correlation radii is approximate only. The a priori error variance is 6 cm^2 (i.e., 15% of an expected signal variance of 40 cm^2). The maps were calculated at regular 10-day intervals from November 20, 1986, through November 20, 1988, in the study domain.

We present in Figure 15 two instantaneous SLA synoptic maps. Figure 15a corresponds to August 20, 1987, and Figure 15b corresponds to January 17, 1988. These are typical of summer and winter conditions, respectively, and allow us to visualize the instantaneous eddy field. Note the well-formed eddies with diameters of about 200 km throughout the northern part of the domain, particularly during winter. These are temporally coherent, as already shown by the correlations, and can be followed over several months. They probably correspond to strong meanders of the Azores current. Note again the larger meridional variance and the tendency of the anomalies to take up a north/south orientation. The wavelike structure of the variability appears clearly, with regular switching between positive and negative anomalies. As can be seen on the longitude time plot of SLA at 34.5°N in Figure 16, propagation velocities are

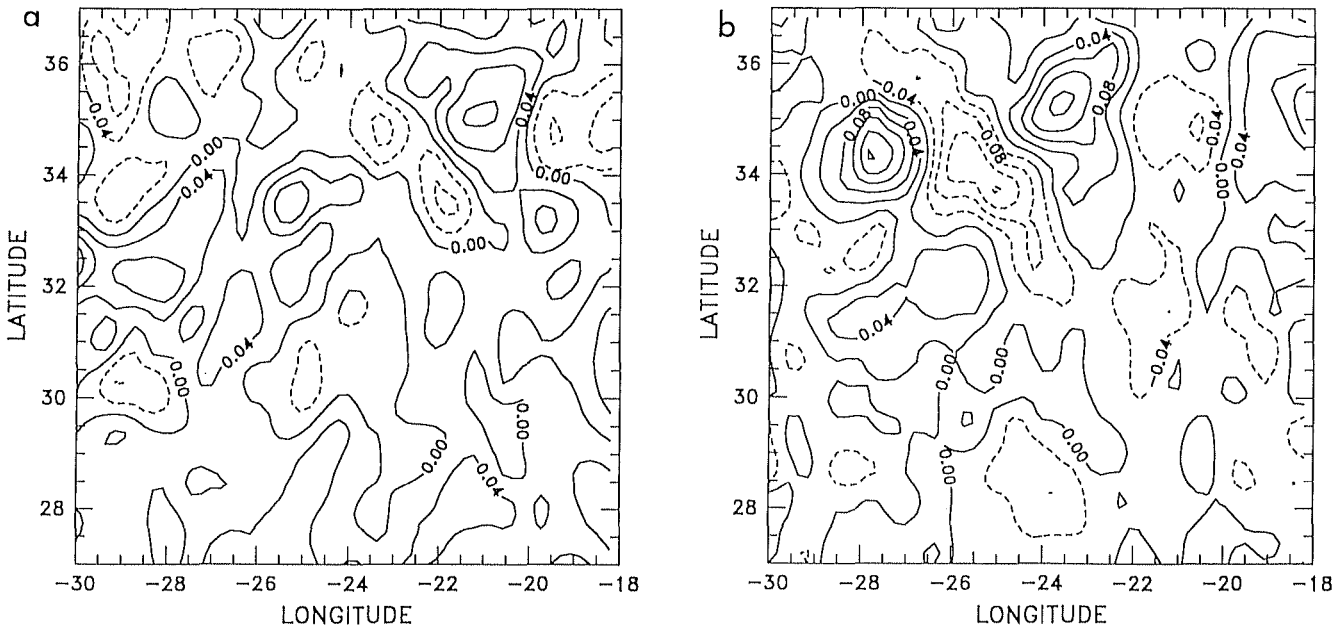

Figure 15. SLA synoptic maps: (a) summer situation, August 20, 1987; (b) winter situation, January 17, 1988. Contour interval is 0.04 m.

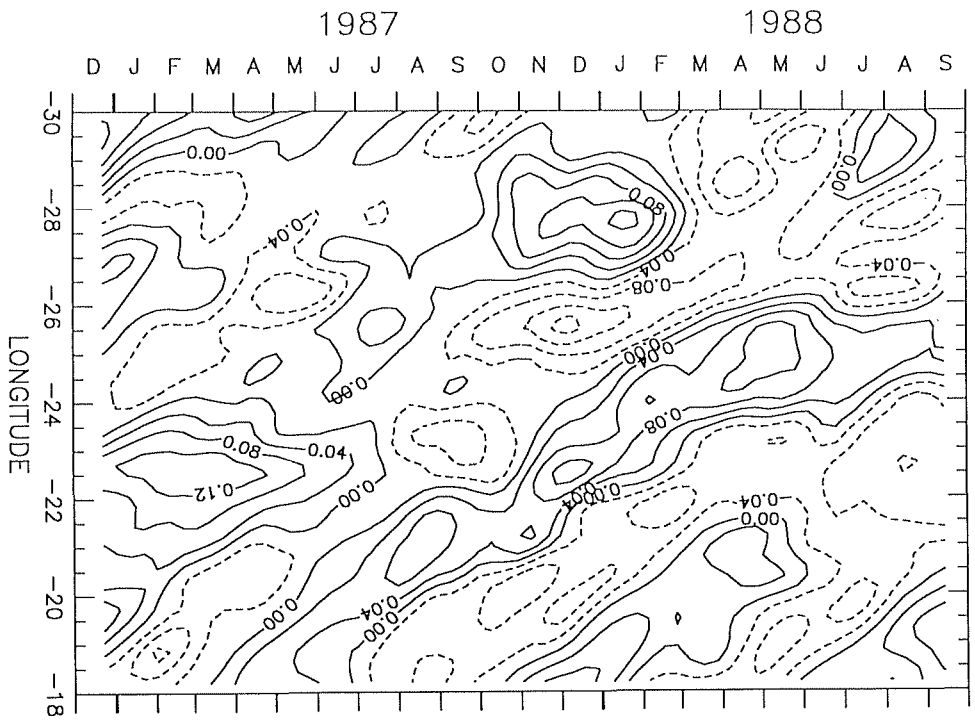

Figure 16. SLA longitude-time plot at 34.5°N. Contour interval is 0.04 m.

westward but slow (1–2 km/d). One can note the disappearance of the features in the western part in summer. These signals are clearly akin to the 250-day and annual signals evidenced in section 4.3. The wavelength of the wave is of about 500 km, and assuming a Rossby wave structure, its group velocity is westward. The features are thus likely to be waves generated in the east which interact with the Azores front in winter and trigger its meandering. In summer these eddies or waves are much less energetic, and the Azores current has a straighter trajectory.

The front seems to penetrate further east in summer. This is visible on the seasonal maps shown on Figure 17. They were calculated by averaging the synoptic maps over a 3-month period and by adding the RBS climatology to get an estimate of the absolute signal. In summer the front is east-west, while in fall/winter it takes a northwest-southeast orientation. These maps can be compared with the seasonal maps obtained by *Stramma and Siedler* [1988] from historical hydrological data which also show a more eastward penetration of the front in summer. In addition, they found a smaller north-south extension of the mean front in summer than in winter. This can be explained by the reduced meandering in summer. We do not, however, observe a southward shift of the front in summer, but this may be masked by the intense winter meandering. Finally, the southward branching appears to occur when the wave in the north interacts with the mean flow, which is consistent with our Reynolds stress analysis.

There are probably several meddies in our study domain [*Armi and Zenk*, 1984], and their interaction with the Azores front does deserve attention. They have a surface signature, and some of them may be present in our SLA synoptic maps [*Käse and Zenk*, 1987; *Stammer et al.*, 1991]. Although some small anticyclonic mesoscale structures may be meddies, they cannot be identified from altimetry alone. In situ data are needed to check their vertical structure.

Recently there has been some concern about the influence of tidal errors on annual signals, mainly because the M2 tide is aliased at about 317 days for Geosat [*Perigaud and Zlotnicki*, 1992; *Cartwright and Ray*, 1990; *Jacobs et al.*, 1992; *Schlax and Chelton*, 1994]. Given the altimeter frequency/wavenumber sampling, the aliased signal has characteristics similar to those of Rossby waves with a 2.3 km/d westward phase propagation at 30°N. However, we do not believe that our results are affected by tidal errors. The procedure to remove the orbit error (first-degree polynomial over 2500 km) also removes the tidal error signal which is strongly correlated along the tracks [e.g., *Schlax and Chelton*, 1994]. Our quasi-annual signal thus has an along-track wavelength of about 600 km, much smaller than what is expected for the tidal signal. Its westward propagation is seen on the along-track frequency/wavenumber spectra and thus does not result from the combination of adjacent tracks polluted by tidal aliasing [*Jacobs et al.*, 1992; *Schlax and Chelton*, 1994]. Furthermore, the dominant period is 250 days with a westward propagation of 1.5 km/d. It is thus significantly different from a tidal error signal (317-day period with a 2.3 km/d propagation). If there is tidal aliasing, one should also see an apparent periodic pattern in the across-track direction. This is not the case, and we see mainly north-south elongated eddies. Finally, recent analyses of ERS 1 data (35-day repeat cycle phase), which have tidal aliasing characteristics different from those of Geosat, show similar westward propagating signals near the Azores frontal area (E. Dombrowsky, personal communication, 1993).

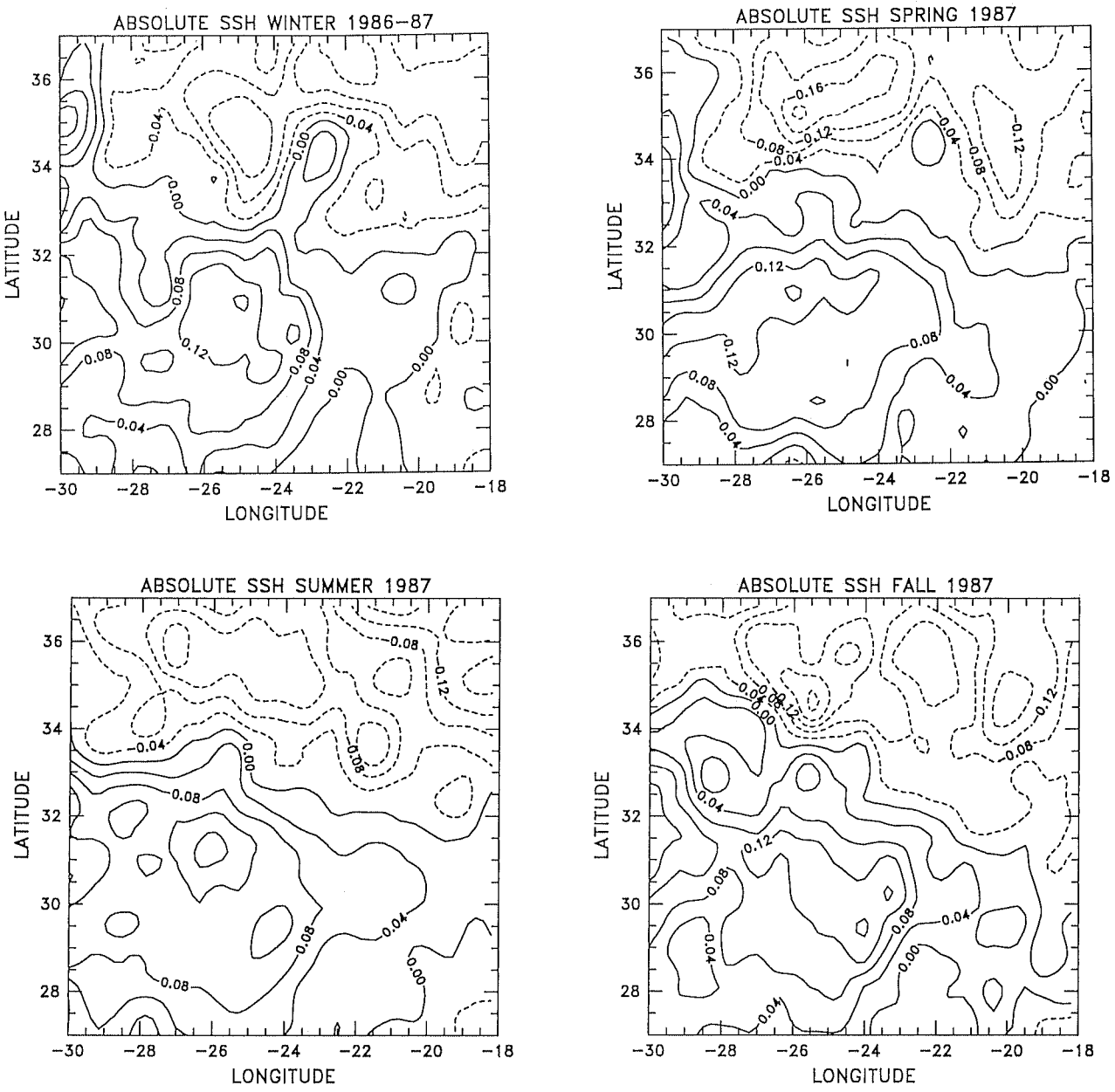

Figure 17. Seasonal averages of synoptic SLA with surface RBS climatology added. Contour interval is 0.04 m.

7. Conclusion

We processed and analyzed 2 years of Geosat altimeter data (November 1986 through November 1988) for the Azores-Madeira area. We carried out a complete statistical and synoptic description of the mesoscale variability for 1986–1988 aimed at describing in detail the dynamics of the Azores-Madeira region. The rms sea surface topography signal varies from 3 to 8 cm. A tongue of maximum variability lies around 34°N. This tongue is linked to the Azores current/front, although it lies north of the mean axis of this current/front. It is characterized by marked anisotropy, with meridional velocity variances two to three times larger than zonal variances. On synoptic maps, the signal appears in the form of strong north-south meanders.

The variability is stronger in winter than in summer and stronger in the second year (1987–1988) than in the first (1986–1987). There is also a clear seasonality in the surface circulation, which is generally consistent with historical in situ measurements. In winter, the current meanders strongly and branches to the south, while in summer it is narrower and penetrates further to the east.

SLA wavenumber spectra have slopes of around −3 for wavelengths less than 350 km and stay red beyond this value. The SLA frequency/wavenumber spectrum shows that the dominant signals have periods larger than 100 days and wavelengths between 300 and 700 km. They have a clear westward propagation. The maximum variability area in the northern part corresponds mainly to signals with periods of 250 days and 1 year. Their wavelike structure is observed on the SLA synoptic maps. The wave has a westward phase and group velocity (assuming a Rossby wave structure). If we accept the fact that the group velocity of the wave is

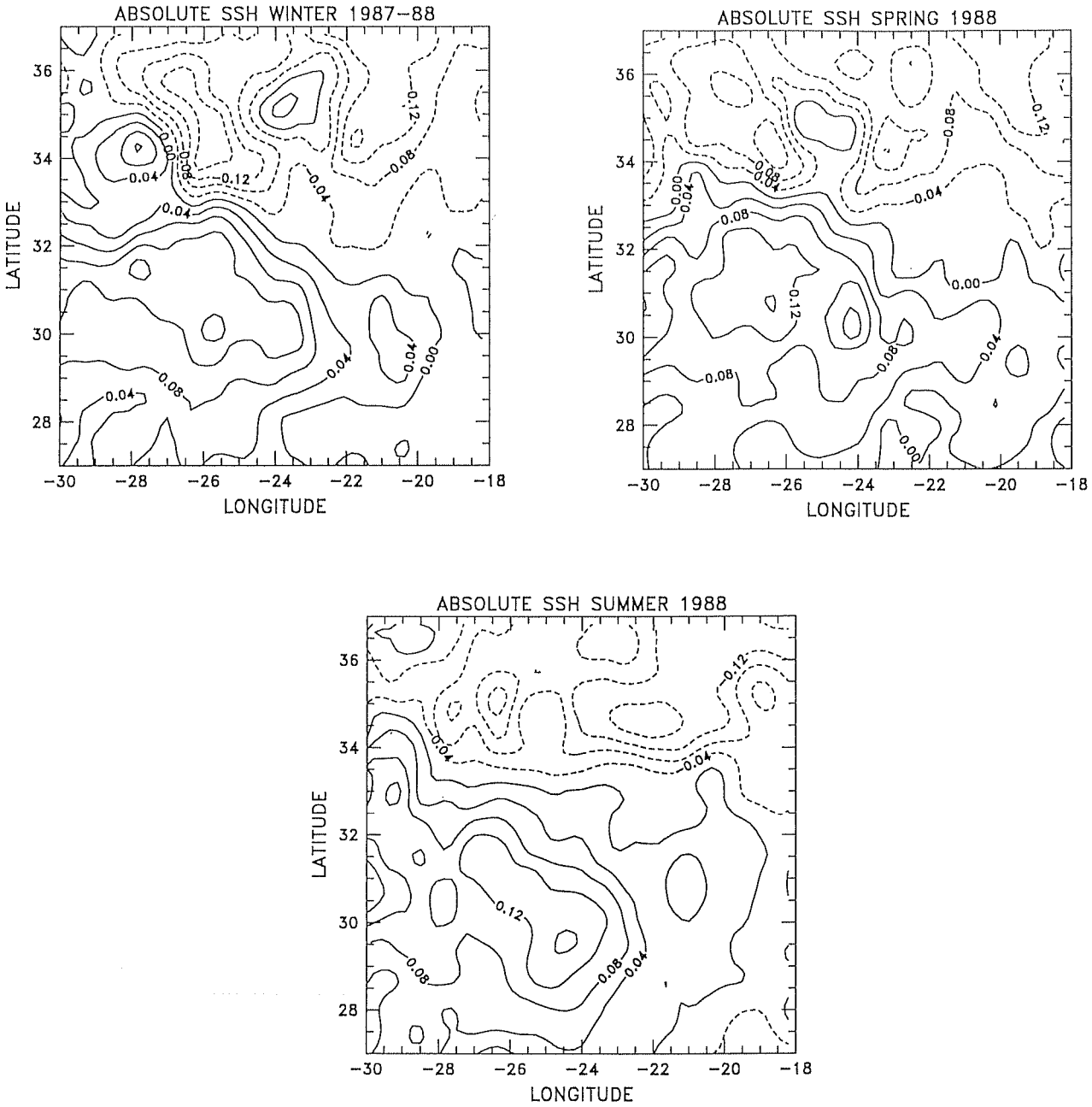

Figure 17. (continued)

westward, then the wave is not generated by the unstable Azores current; it is generated more to the east. This is consistent with the large relative variance of the 250-day-period signal east of 20°W. The wave interacts with the front in winter and forms meanders, while being slowed down in its propagation.

Finally, most changes in direction and strength of the mean flow are consistent with momentum transfers from the turbulent field to the mean. In addition, torques due to Reynolds stresses in the western part seem to work directly within the axis of the current, with the result that meanders are created there; more to the east, the net zonal acceleration vanishes, a branch of the mean current veers to the south, and the meanders take the form of waves centered at 34°N.

Acknowledgments. We thank J. F. Minster and X. Carton for their useful comments. The Geosat data set was provided by GRGS/UMR39. This study was partly supported by GERDSM-CLS contract A 92 48 648 000.

References

Arhan, M., and A. Colin de Verdière, Dynamics of eddy motions in the eastern North Atlantic, *J. Phys. Oceanogr.*, *15*, 153–170, 1985.

Armi, L., and W. Zenk, Large lenses of highly saline Mediterranean water, *J. Phys. Oceanogr.*, *14*, 1560–1576, 1984.

Böning, C. W., and R. G. Budich, Eddy dynamics in a primitive equation model: Sensitivity to horizontal resolution and friction, *J. Phys. Oceanogr.*, *22*, 361–381, 1991.

Cartwright, D. E., and R. D. Ray, Oceanic tides from Geosat altimetry, *J. Geophys. Res.*, *95*, 3069–3090, 1990.

Cheney, R. E., B. C. Douglas, R. W. Agreen, L. Miller, D. L. Porter, and N. S. Doyle, *Geosat Altimeter Geophysical Data Record User Handbook*, National Ocean Service, NOAA, Rockville, Md., 1987.

De Mey, P., Synoptic estimates of an eddy field in the North Atlantic current, *Oceanol. Acta*, *15*, 537–543, 1992.

De Mey, P., and Y. Ménard, Synoptic analysis and dynamical adjustment of Geos 3 and Seasat altimeter eddy fields in the North West Atlantic, *J. Geophys. Res.*, *94*, 6221–6230, 1989.

Emery, W. J., W. G. Lee, and L. Magaard, Geographic and seasonal distributions of Brunt Väisälä frequency and Rossby radii in the North Pacific and North Atlantic, *J. Phys. Oceanogr.*, *14*, 294–317, 1984.

Eymard, L., et al., The SEMAPHORE mesoscale air-sea experiment (1993), technical report, Cent. de Rech. sur la Phys. de l'Environ., Issy-les-Moulineaux, France, 1991.

Flierl, G. R., P. Malanotte-Rizzoli, and N. J. Zabusky, Nonlinear waves and coherent vortex structures in barotropic beta-plane jets, *J. Phys. Oceanogr.*, *17*, 14,108–14,138, 1987.

Gould, W. J., Physical oceanography of the Azores front, *Prog. Oceanogr.*, *14*, 167–190, 1985.

Haines, B. J., G. H. Born, G. W. Rosborough, J. G. Marsh, and R. G. Williamson, Precise orbit computation for the Geosat exact repeat mission, *J. Geophys. Res.*, *95*, 2871–2886, 1990.

Hua, B. L., and D. B. Haidvogel, Numerical simulations of the vertical structure of quasi-geostrophic turbulence, *J. Atmos. Sci.*, *43*, 2923–2936, 1986.

Ikeda, M., Meanders and detached eddies of a strong eastward flowing jet using a two layer quasi-geostrophic model, *J. Phys. Oceanogr.*, *11*, 526–540, 1981.

Jacobs, G. A., G. H. Born, M. E. Parke, and P. C. Allen, The global structure of the annual and semiannual sea surface height variability from Geosat altimeter data, *J. Geophys. Res.*, *97*, 17,813–17,828, 1992.

Jourdan, D., C. Boissier, A. Braun, and J. F. Minster, Influence of wet tropospheric correction on mesoscale dynamic topography as derived from satellite altimetry, *J. Geophys. Res.*, *95*, 17,993–18,004, 1990.

Käse, R. H., and G. Siedler, Meandering of the subtropical front south-east of the Azores, *Nature*, *300*, 245–246, 1982.

Käse, R. H., and W. Zenk, Reconstructed Mediterranean salt lens trajectory, *J. Phys. Oceanogr.*, *17*, 185–193, 1987.

Käse, R. H., W. Zenk, T. B. Sanford, and W. Hiller, Currents, fronts and eddy fluxes in the Canary basin, *Prog. Oceanogr.*, *14*, 231–257, 1985.

Käse, R. H., J. F. Price, P. L. Richardson, and W. Zenk, A quasi-synoptic survey of the thermocline circulation and water mass distribution within the Canary basin, *J. Geophys. Res.*, *91*, 9739–9748, 1986.

Kielmann, J., and R. H. Käse, Numerical modeling of meander and eddy formation in the Azores current frontal zone, *J. Phys. Oceanogr.*, *17*, 529–541, 1987.

Klein, B., and G. Siedler, On the origin of the Azores current, *J. Geophys. Res.*, *94*, 6159–6168, 1989.

Krauss, W., and C. W. Böning, Lagrangian properties of eddy fields in the northern North Atlantic as deduced from satellite-tracked buoys, *J. Mar. Res.*, *45*, 259–291, 1987.

Krauss, W., and R. H. Käse, Mean circulation and eddy kinetic energy in the eastern North Atlantic, *J. Geophys. Res.*, *89*, 3407–3415, 1984.

Le Traon, P. Y., Time scales of mesoscale variability and their relationship with spatial scales in the North Atlantic, *J. Mar. Res.*, *49*, 467–492, 1991.

Le Traon, P. Y., Contribution of satellite altimetry to the observation of the mesoscale oceanic variability, *Oceanol. Acta*, *15*, 437–451, 1992.

Le Traon, P. Y., and F. Hernandez, Mapping the oceanic mesoscale variability: Validation of satellite altimetry using surface drifters, *J. Atmos. Oceanic Technol.*, *9*, 687–698, 1992.

Le Traon, P. Y., M. C. Rouquet, and C. Boissier, Spatial scales of mesoscale variability in the North Atlantic as deduced from GEOSAT data, *J. Geophys. Res.*, *95*, 20,267–20,285, 1990.

Le Traon, P. Y., C. Boissier, and P. Gaspar, Analysis of errors due to polynomial adjustments of altimeter profiles, *J. Atmos. Oceanic Technol.*, *8*, 385–396, 1991.

Maillard, C., and R. H. Käse, The near surface flow in the subtropical gyre south of the Azores, *J. Geophys. Res.*, *94*, 16,133–16,140, 1989.

Mercier, H., and A. Colin de Verdière, Space and time scales of mesoscale motions in the eastern North Atlantic, *J. Phys. Oceanogr.*, *15*, 171–183, 1985.

Minster, J. F., D. Jourdan, E. Normant, C. Brossier, and M. C. Gennero, An improved SSM/I water vapor correction for Geosat altimeter data, *J. Geophys. Res.*, *97*, 17,859–17,872, 1992.

Morrow, R., Surface eddy variability and eddy momentum flux in the southern ocean from Geosat altimetry, Ph.D. thesis, 250 pp., Univ. of Sydney, Sydney, Australia, 1992.

Morrow, R., J. Church, R. Coleman, D. Chelton, and N. White, Eddy momentum flux and its contribution to the southern ocean momentum balance, *Nature*, *357*, 482–484, 1992.

Müller, T. J., and G. Siedler, Multi-year current time series in the North Atlantic ocean, *J. Mar. Res.*, *50*, 63–98, 1994.

Parke, M. E., R. H. Stewart, D. L. Farless, and D. E. Cartwright, On the choice of orbits for an altimetric satellite to study ocean circulation and tides, *J. Geophys. Res.*, *92*, 11,693–11,707, 1987.

Perigaud, C., and V. Zlotnicki, Importance of Geosat orbit and tidal errors in the estimation of large-scale Indian ocean variations, *Oceanol. Acta*, *15*, 491–506, 1992.

Robinson, M. K., R. A. Bauer, and E. H. Schroeder, Atlas of North Atlantic-Indian ocean monthly mean temperature and mean salinities of the surface layer, *Ref. Publ. 18*, U.S. Naval Oceanogr. Office, Washington, D. C., 1979.

Schlax, M. G., and D. B. Chelton, Detecting aliased tidal errors in altimeter height measurements, *J. Geophys. Res.*, in press, 1994.

Schmitz, W. J., J. F. Price, and P. L. Richardson, Recent moored current meter and SOFAR float observations in the eastern Atlantic near 32°N, *J. Mar. Res.*, *46*, 301–319, 1988.

Siedler, G., W. Zenk, and W. J. Emery, Strong current events related to a subtropical front in the Northeast Atlantic, *J. Phys. Oceanogr.*, *15*, 885–897, 1985.

Spall, M. A., Circulation in the Canary basin: A model/data analysis, *J. Geophys. Res.*, *95*, 9611–9628, 1990.

Stammer, D., H. H. Hinrichsen, and R. H. Käse, Can meddies be detected by satellite altimetry?, *J. Geophys. Res.*, *96*, 7005–7014, 1991.

Stramma, L., and G. Siedler, Seasonal changes in the North Atlantic subtropical gyre, *J. Geophys. Res.*, *93*, 8111–8118, 1988.

Sy, A., Investigation of large-scale circulation patterns in the central North Atlantic: The North Atlantic current, the Azores current, and the Mediterranean water plume in the area of the Mid-Atlantic ridge, *Deep Sea Res.*, *35*, 383–413, 1988.

Tai, C. K., and W. B. White, Eddy variability in the Kuroshio Extension as revealed by Geosat altimetry: Energy propagation away from the jet, Reynolds stress, and seasonal cycle, *J. Phys. Oceanogr.*, *20*, 1761–1777, 1990.

Tokmakian, R. T., and P. G. Challenor, Observations in the Canary basin and the Azores frontal region using Geosat data, *J. Geophys. Res.*, *98*, 4761–4773, 1993.

P. De Mey, Groupe de Recherches de Géodésie Spatiale, UMR39, 18 Avenue Edouard Belin, 31055 Toulouse Cedex, France.

P.-Y. Le Traon, CLS Space Oceanography Group, 18 Avenue Edouard Belin, 31055 Toulouse Cedex, France.

(Received August 30, 1993; revised December 14, 1993; accepted December 14, 1993.)